Study and Characterization of Optoelectronic Photoconductor-Based Probes

Robert H. Voelker, *Senior Member, IEEE*, Michael Y. Frankel, and Christopher G. Sentelle

Abstract— **Photoconductor sampling probes are important for optoelectronic device and circuit measurement applications. We use the finite-difference transmission line matrix (FD-TLM) method to characterize the ultrafast photoconductor sampling probes' fundamental performance limits imposed by electromagnetic constraints. Both on-wafer and free-standing photoconductor probes are investigated as applied to microstrip lines found in millimeter-wave integrated circuits and as applied to coplanar strip lines found in ultrafast device characterization systems. Localized invasiveness, distributed loading, and measurement accuracy are investigated for various probing configurations and orientations. Localized invasiveness is small for all our simulations. Distributed loading is negligible for cases where the guided-mode field confinement is tighter than the spatial separation between the probe support structure and the transmission line. Measurement accuracy is acceptable for simulated structures, but amplitude calibration precision may be compromised. We also study photoconductor probes for high-bandwidth signal generation on transmission line structures. The generated signals follow the photoconductor switch photocurrent signal for cases where both the probe and the transmission line form well-matched guiding-wave structures but are attenuated and distorted for other cases.**

I. Introduction

PHOTOCONDUCTOR (PC) sampling probes are important for device and circuit measurement applications. The integrated on-wafer PC probe concept has been developed in detail by Auston [1] as applied to microstrip (MS) transmission lines. The response of the on-wafer PC microstrip sampling probe has been explored based on a lumped-element approach, with the emphasis placed on accounting for the PC switch response limitations. Such approach is expected to be accurate for the MS transmission lines with bandwidths constrained by the mechanical substrate thickness. The MS transmission lines, combined with integrated on-wafer sampling and generation probes, have been used in a many applications from microwave signal generation [1] to high-bandwidth characterization of transistors [2], [3] and circuits [4]. The PC sampling technique has been extended to wide-bandwidth photolithographically-defined coplanar strip (CPS) transmission lines with on-wafer probe geometries which need to reproduce signals with frequency components up to roughly one terahertz [5]. The lumped element approach to evaluating the response of a PC probe on CPS lines is unlikely to produce accurate results at such frequencies.

Integrated on-wafer PC probe structures require substantial substrate area and are unable to be repositioned. Consequently, considerably more flexible free standing photoconductor probes have been developed and applied to measurements on MS and CPS lines at arbitrary points [6]–[8]. Free standing probe measurement linearity and sensitivity are determined primarily by the photoconductor switch response and have been explored experimentally [9]. The distributed loading of the CPS lines due to the probe support structure has been investigated experimentally also [9]. However, the localized and distributed effects of the PC probe on the signal propagating on the MS and CPS transmission lines and the accuracy with which the actual propagating signal is measured have not been explored quantitatively. Addressing such issues is important if the free-standing probes are to reach their full potential as flexible instruments for high-speed signal measurement in microwave and millimeter-wave devices and circuits, and if they are to find wider uses outside of the research laboratory.

We use the finite-difference transmission line matrix (FD-TLM) [10] numerical technique to investigate the fundamental limits placed by electromagnetic effects on the performance of both on-wafer and free-standing PC probes. The effects of the PC switch itself have been explored in detail by others and will not be considered here [1], [8], [9], [11], and [12]. Section II presents and discusses the performance of on-wafer probes as high-bandwidth signal measurement and generation tools. Much experimental data is available in the literature for on-wafer configurations that validate the FD-TLM results and provide a baseline for comparisons to free-standing probes. Section III presents and discusses the performance of free-standing photoconductor probes.

II. FD-TLM Simulation of MS and CPS with On-Wafer Probe

The FD-TLM full-wave time-domain numerical method solves for electromagnetic fields at nodes situated on a graded rectangular mesh of transmission lines in three-dimensional space [10]. There is a one-to-one correspondence between the FD-TLM nodes and points in the structure being simulated. It is important to note that although space is discretized into cells by transmission lines, completely arbitrary guiding and nonguiding structures discretized on a graded rectangular mesh can be modeled by the FD-TLM method. Good agreement between FD-TLM simulations and experiments on coplanar

Manuscript received January 15, 1995, revised November 12, 1995. This work was supported in part by the Center for Electro-Optics of the University of Nebraska-Lincoln and the Office of Chief of Naval Research.

R. H. Voelker and C. G. Sentelle are with the Department of Electrical Engineering and Center for Electro-Optics, University of Nebraska-Lincoln, Lincoln, NE 68588-0511 USA.

M. Y. Frankel is with CODE 5672, Optical Sciences Division, Naval Research Laboratory, Washington, DC 20375-5338 USA.

Publisher Item Identifier S 0018-9480(96)01456-1.

striplines at frequencies up to hundreds of gigahertz [13] demonstrates the suitability of the FD-TLM method for modeling structures discussed here. Limitations on the accuracy of the FD-TLM simulations are numerical dispersion and resolution of the conductor widths. Numerical dispersion is minimized by using an FD-TLM grid spacing no larger than a tenth of a wavelength for the highest frequency signals propagating along the structure [13]. The conductor widths are well resolved by using for the 70-μm-wide MS 25 cells with grid spacing as small as 2 μm, and for the 10-μm-wide CPS conductors, five cells with a 2 μm grid spacing. FD-TLM modeling techniques such as pulse excitation of guided-wave structures and calculation of guided-wave voltages, currents, and frequency-dependent impedance, attenuation, and effective relative permittivity are discussed in [13]. The conductors are assumed to be ideal in all our simulations, but resistive effects could also be included at the expense of significant additional computer resources. Since this effort concentrates on localized and distributed electromagnetic coupling effects rather than attenuation caused by resistive effects, perfect conductors are used in the simulations.

To validate FD-TLM modeling of optoelectronic photoconductor samplers, simulations of an MS and a CPS with an on-wafer sampling probe are performed for which much experimental data is available. The 50-Ω MS in Fig. 1(a) is first simulated without the PC probe to verify proper modeling of the MS itself. The 70-μm-wide MS, as well as all conductors in the simulations presented, is modeled as an infinitesimally-thick, perfectly-conducting material. The MS left edge is positioned 1.007 mm from the left wall of the perfectly-conducting rectangular box of size $2.794 \times 0.608 \times 5.884$ mm^3 (x, y, z). At the front of the box on the 0.1-mm-thick GaAs substrate is the E_z electric field excitation which develops a 1-V peak amplitude, 3.25-ps full-width at half-maximum (FWHM) Gaussian pulse. A 50-Ω resistor modeled as a lossy conductor is in series with the excitation to drive the MS, and roughly halves the actual injected signal. A 50-Ω load resistor terminates the MS far end to the ground plane.

Fig. 2 compares the frequency-dependent MS effective relative permittivity calculated from MS voltages at 0.225 mm and 1.475 mm from the box front with the effective permittivity from a semi-empirical dispersion formula [14]. Good agreement for all frequencies up to 300 GHz validates the FD-TLM MS propagation modeling. The large variation in the effective permittivity, even at comparatively low frequencies, indicates the highly dispersive nature of the MS. Also, no signal attenuation is observed in the FD-TLM results, in accordance with the expected absence of attenuation assuming perfect conductors.

The PC sampling probe is modeled as a 70-μm-wide, 50-Ω probe MS placed 10 μm from the right edge of the main MS [Fig. 1(a)]. The probe MS, on top of the substrate, is spaced 2.907 mm from the front of the box to provide sufficient temporal separation between the incident pulse and the pulse reflected by the probe discontinuity (Fig. 3). The localized invasiveness of the PC probe is evaluated from the incident and reflected pulses traveling along the main MS which are calculated 1.725 mm from the front wall and are plotted in

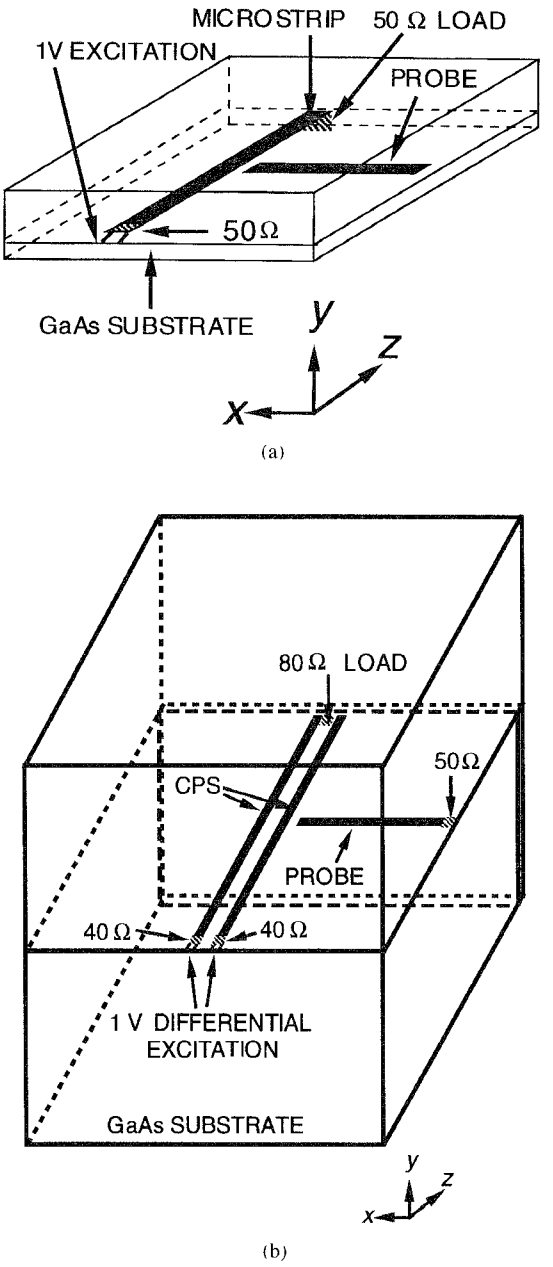

Fig. 1. Layouts of simulated structures. (a) Microstrip and (b) coplanar stripline.

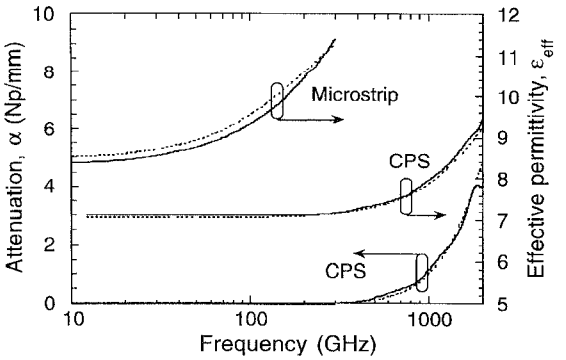

Fig. 2. Transmission line propagation characteristics calculated from FD-TLM simulations (solid lines) and analytic semi-empirical formulas (dotted lines).

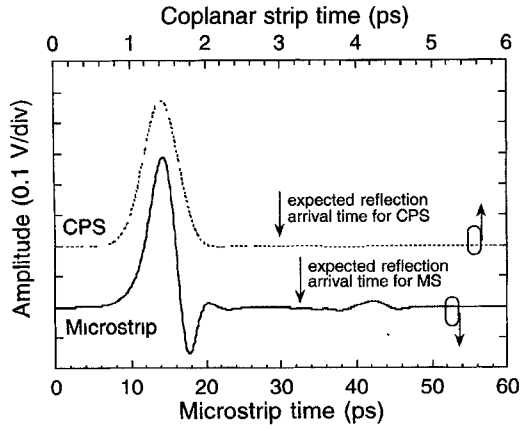

Fig. 3. Incident and reflected voltages on the main line due to the integrated on-wafer probe for the MS (solid) and the CPS (dotted) lines.

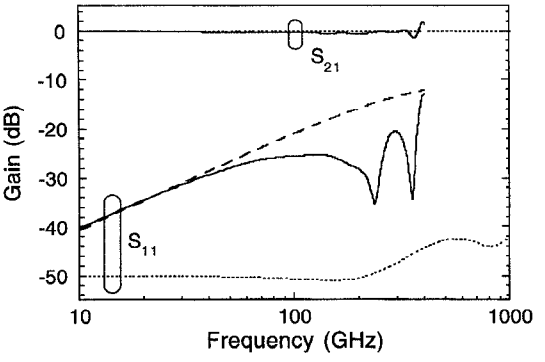

Fig. 4. Reflection (S_{11}) and transmission (S_{21}) S-parameters due to the integrated on-wafer probe for the MS (solid) and the CPS (dotted) lines. The dashed line is an S_{11} parameter calculated assuming a microstrip probe line coupled to the main MS line by a 6-fF capacitor.

Fig. 3. The pulse transmitted past the probe is calculated 8 μm from the probe edge. By windowing the incident, reflected, and transmitted pulses in the time domain, performing an FFT on each, and then calculating the ratios, S-parameters S_{11} and S_{21} are determined (Fig. 4). Fig. 4 shows S_{11} and S_{21} for the probe structure near the MS. Ripple in the MS S_{11} is caused by higher-order non-TEM modes at about 230 and 350 GHz being excited by the probe discontinuity. This conclusion is supported by a ripple observed to develop on the reflected signal in the time domain. The dashed line, coinciding with the FD-TLM results at low frequencies and following the overall envelope at higher frequencies, is developed from a simple model consisting of a main MS with a probe MS coupled via a 6-fF capacitor. Also in Fig. 4 is the FD-TLM-calculated MS S_{21} which is very close to 0 dB, indicating that the sampling probe has little effect on the transmitted signal.

Fig. 5 shows the actual MS voltage calculated at the location of the sampling probe and the voltage calculated across the sampling probe gap. The actual MS pulse is dispersed, as expected from the Fig. 2 data, with trailing ripples indicating the reduced velocity at high frequencies. The probe gap voltage represents the signal that would be measured by a PC switch with an ideal instantaneous response, providing an amount of charge to the detection electronics that is proportional to the voltage across the gap at the time defined by the

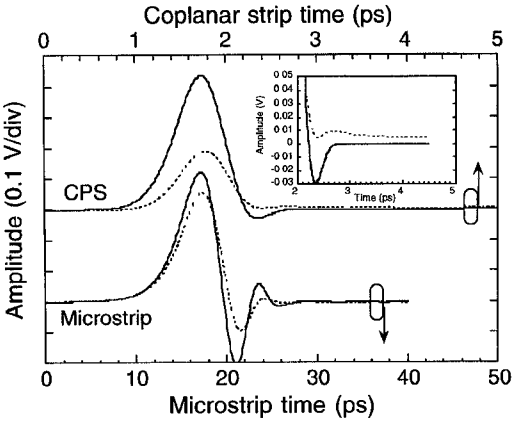

Fig. 5. Actual transmission line guided-mode voltages (solid) and the voltages across the on-wafer probe gap (dotted). The inset shows the long tail present across the CPS on-wafer probe gap.

optical sampling impulse trigger. The actual current signal is determined by semiconductor switch parameters which ideally set a constant of proportionality between gap voltage and current. The gap voltage follows the actual MS voltage with a slightly reduced amplitude and with only a minor loss of high frequency information signified by somewhat reduced trailing ripples, supporting the accuracy of many PC sampling measurements on MS lines that have been reported [1]–[4]. The probe frequency response cancels in those measurements that rely on taking the frequency-domain ratio of measured signals, for example as is done for device S-parameter measurements [4].

The performance of the PC probe as a generator of signals on the main MS is also investigated. Such signal generation may be useful for applications in device and circuit characterization. Fig. 6 shows the MS voltage at a point 4 μm from the probe edge as a result of a 20 mA peak amplitude, 3.25-ps FWHM Gaussian current pulse injected by the PC switch gap. The current-source pulse generation, rather than the voltage-source, is believed to better represent the actual PC switch behavior. A current source is created by exciting the magnetic fields in a small loop closely surrounding the PC gap. The current induced in the gap is equal to the line integral of the magnetic field around the loop. A voltage source is created by exciting the longitudinal electric field between the ends of the metal conductors in the PC gap. The gap voltage is then equal to the line integral of the electric field. Under ideal circumstances, and assuming a 50-Ω MS impedance, such generation should produce a 0.5-V-peak propagating voltage pulse. The well-behaved generated signal has nearly negligible ripples following the main Gaussian pulse which is identical to the behavior in experimental data reported in the literature and validates the applicability of the on-wafer photoconductor probe signal generation on MS lines.

The same type of FD-TLM simulations performed on the MS are also performed on the CPS structure shown in Fig. 1(b). The 10-μm-wide CPS conductors are separated by 10 μm and are mounted on a 0.2-mm-thick GaAs substrate to form an approximately 80-Ω line. The E_z electric fields are excited in the gaps between the 40-Ω resistors and the front

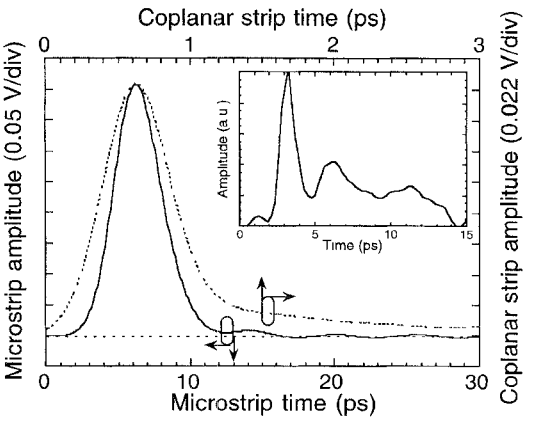

Fig 6. Voltages generated via an on-wafer probe on the MS (solid) and the CPS (dotted) lines. The inset shows a typical experimentally-measured signal generated on a CPS line via an on-wafer probe

wall to create a differential 1-V peak amplitude, 0.5-ps FWHM Gaussian pulse, with the source resistance approximately halving the actual injected signal. At the other end of the CPS, an 80-Ω load resistor is implemented to reduce reflections. The left CPS conductor is spaced 0.2 mm from the left box wall. The rectangular GaAs substrate extends to within 8 μm of the rear of the $0.442 \times 0.408 \times 0.42$ mm^3 (x, y, z) perfectly-conducting shielding box.

Fig. 2 shows the frequency-dependent CPS effective relative permittivity and attenuation calculated from voltages between the CPS conductors at 68 μm and 108 μm from the front wall. For comparison, the effective permittivity and the attenuation based on semi-empirical analytic formulas [15] are also shown. Compared with the MS, the CPS line shows negligible dispersion up to 400 GHz indicating an order of magnitude bandwidth improvement. However, the attenuation, which is dominated by radiative losses, is present even for an ideal conductor case and is rapidly increasing at higher frequencies [15]. Good agreement between FD-TLM simulation and the experimentally-verified formulas for all frequencies up to 2 THz validates the FD-TLM CPS modeling.

Fig. 3 shows the pulse incident toward and the negligible reflected pulse from the 10-μm-wide sampling probe MS mounted 10 μm from the right CPS conductor and 0.204 mm from the front wall (Fig. 1(b)). The time scale for the CPS simulation in Fig. 3 is an order of magnitude shorter than for the MS simulation. From Fig. 3, it is clear that the discontinuity presented by the on-wafer probe structure to the CPS is much smaller than the on-wafer probe discontinuity presented to the MS, even considering that the CPS signal bandwidth is an order of magnitude larger. This is expected since the probe structure for the CPS is high-impedance and is only weakly coupled to the guided mode which is primarily confined between the CPS electrodes, whereas the probe structure for the MS appears as a low impedance MS line capacitively coupled to the main line.

Fig. 4 shows the frequency-domain S_{11} and S_{21} for the sampling probe structure on the CPS. Again, the smaller S_{11} of the CPS compared with the MS S_{11} indicates that the sampling probe has less effect on the CPS performance than on the MS performance. The actual S_{11} magnitude for the CPS case may be smaller than indicated since only four significant digits of the double-precision FD-TLM numerical results are used when performing the FFT. The transmitted voltage pulse is calculated 12 μm from the probe edge, and the S_{21} deviates negligibly from 0 dB over the whole 1-THz frequency range indicating negligible transmitted pulse loss.

Fig. 5 shows the actual CPS voltage calculated at the location of the sampler probe and the voltage calculated in the sampler probe gap. The time scale for the CPS waveform is an order of magnitude shorter than for the MS one. The CPS has a smaller ratio of gap voltage to transmission line voltage than does the MS, indicating that the sampling probe is less effective at measuring CPS voltages than MS voltages. The bandwidth of the PC switch gap signal compared with the actual one is somewhat reduced, as manifested by the reduced trailing ripple. A more significant parasitic effect appears as a long positive tail in the probe gap voltage (inset, Fig. 5), which may invalidate low-frequency calibration procedures as well as introduce deleterious truncation errors when performing FFT's. This effect is attributed to a slow discharge of the parasitic probe capacitance and the high effective impedance of the probe line structure.

Fig. 6 shows a CPS voltage calculated 16 μm from the probe conductor edge produced by a 12.5 mA peak amplitude, 0.5-ps FWHM Gaussian current pulse generated by the PC switch gap. Under ideal circumstances, and assuming an 80-Ω CPS impedance, such generation should produce a 0.5-V-peak propagating voltage pulse. The amplitude for the CPS signal is a factor of 2.25 smaller than for the MS indicating a significantly less efficient signal generation on the CPS by the on-wafer probe. Furthermore, a long positive shoulder is observed to form following the initial pulse. The fundamental difference between the two cases appears to be that the MS generation takes place from a guiding-wave structure which is well matched to the main MS, while the CPS generation takes place from a relatively high-impedance unguiding structure completely unmatched to the main CPS.

The inset of Fig. 6 shows an experimentally-measured signal generated via an on-wafer PC probe into a CPS line. The experimental arrangement is similar to that shown in Fig. 1(b). A dc bias is applied to the PC probe line and the PC switch gap is excited by a 100-fs laser pulse. The electrical signal injected into the CPS line is measured by an electro-optic sampling technique with sub-picosecond time resolution [17]. Whereas we expect a single-picosecond-pulse response, the observed waveform is followed by a long positive shoulder in qualitative agreement with simulations. In contrast, clean single-picosecond-pulses can be easily generated on the CPS line via a *guiding-wave* on-wafer probe structure [17].

III. FD-TLM Simulation of MS and CPS with Free-Standing Probes

The successful FD-TLM modeling of MS and CPS with the on-wafer integrated samplers leads next to modeling of these lines with free-standing sampling probes. Fig. 7 shows the construction of such probes, with probe length L, width

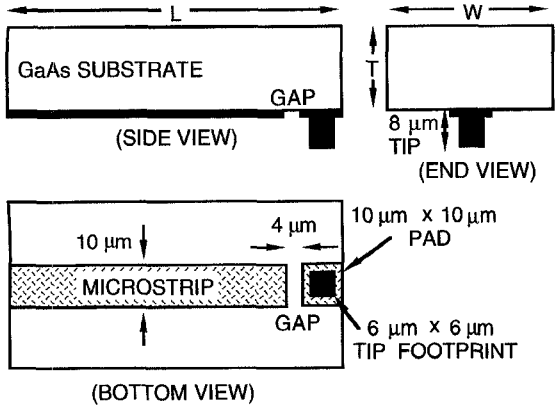

Fig. 7. Side, end, and bottom views of free-standing probe geometry.

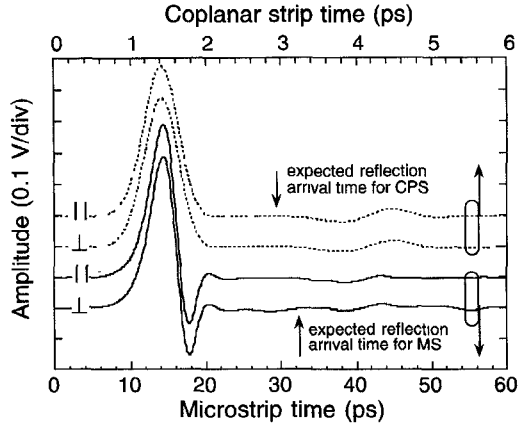

Fig. 8. Incident and reflected voltages on the main line due to the free-standing probes with parallel and perpendicular orientation on the MS (solid) and the CPS (dotted) lines.

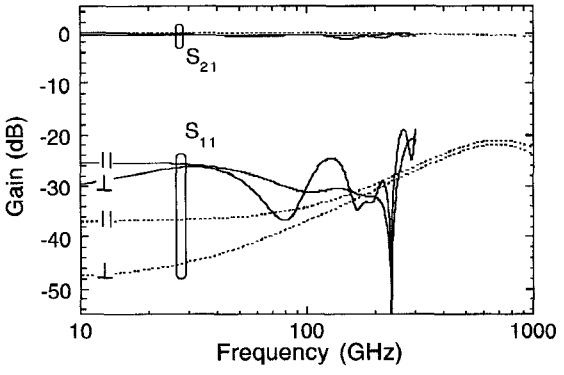

Fig. 9. Reflection (S_{11}) and transmission (S_{21}) S-parameters due to the free-standing probes for the MS (solid) and the CPS (dotted) lines.

W, and thickness T. In the simulations, the probe substrate thickness T extends to the top of the shielding box. The top of the box serves as the ground plane for the MS of the free-standing probes. All probes have in common a solid tip mounted on a pad which is separated from a narrow microstrip by a PC gap. In FD-TLM modeling of the probes, the probe tip, touching the metal conductor, is centered along the width of the metal transmission line at the same distance from the front wall as the on-wafer probe in the original simulations. During the simulations, the probe's support arm substrate length L is either perpendicular to the main transmission line and over the substrate area where the on-wafer probe was once located ("perpendicular" orientation) or parallel to the main transmission line directly over the conductors and extending toward the load resistor ("parallel" orientation).

The FD-TLM simulations of Section II are repeated with the free-standing probes in perpendicular and parallel orientations replacing the on-wafer probe. The perpendicular probe support arm substrate used for MS sampling is 0.984 mm wide (W) and its length L extends to the right box wall, while the parallel probe support arm substrate has a width of 0.994 mm and length extending to the rear wall. The perpendicular probe for CPS measurements has support arm substrate width W extending from the front to back box walls and length L extending to the right wall, and the parallel probe support arm substrate width spans from the left to right walls and its length reaches the rear wall.

Fig. 8 shows the incident and reflected signals according to probe orientation and transmission line type. The signals are calculated at the same positions along the main transmission line as when the on-wafer probe was used. The 1-V peak amplitude Gaussian pulses used for each simulation are 3.25 ps FWHM for the MS and 0.5 ps FWHM for the CPS. For the MS line, the signal reflected from the free-standing probe is similar in amplitude to the reflection produced by the on-wafer probe, indicating a similar magnitude discontinuity. In contrast, the reflection produced by the free-standing probe on the CPS line is considerably larger than in the on-wafer probe case, and approaches the MS reflection in amplitude. This is caused by the presence of the free-standing probe dielectric immediately above the CPS line electrodes and a concomitant distortion of the guided mode field distribution leading to reflection.

Fig. 9 shows the frequency-domain S_{11} and S_{21} plotted according to free-standing probe orientation and transmission line type. As previously indicated, the reflections from the free standing probes on the MS and CPS are comparable in amplitude, especially at higher frequencies. However, these reflections are still sufficiently small to cause acceptably small errors in most applications. The nearly 0 dB S_{21} for all combinations indicates that the probe contacts have little effect on the signal propagating past the probes and that the localized invasiveness is small.

In addition to the localized effect of the probe contact itself, there is also a distributed effect of the free-standing probe dielectric in the parallel configuration. In Fig. 10 we compare the voltage signal at the terminating resistance for the transmission lines with no probe loading to the voltage signal obtained with the parallel probe loading and observe a substantial dielectric loading and a corresponding signal delay in the MS case. The signal delay of 3.54 ps is induced by the propagation under the 2.9-mm-long MS section capped by a probe superstrate. There is also some minor signal amplitude reduction primarily due to the reflection loss at the probe contact (see S_{21}, Fig. 9). In the CPS case, the probe contact induces some high-frequency losses as well (see S_{21}, Fig. 9), but there appears almost no measurable delay induced by the 210-μm-long superstrate overlap. The experimental

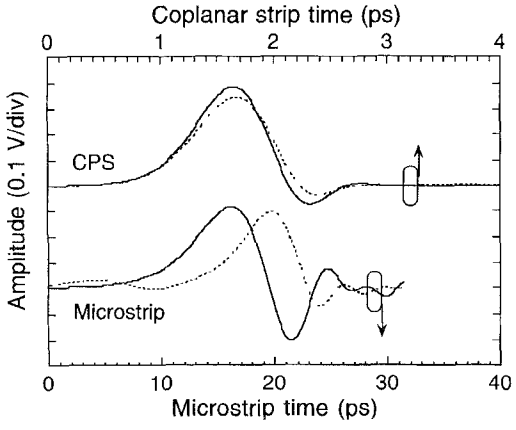

Fig. 10. Guided-mode signal propagation on unperturbed (solid) and parallel-probe loaded (dotted) main transmission lines.

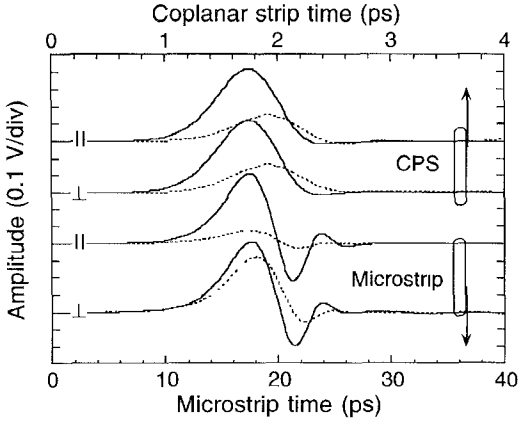

Fig. 11. Actual transmission line guided-mode voltages (solid) and the voltages across the free-standing probe gap (dotted).

measurements reported in the literature [9], [18] do show some probe-induced delay for the CPS lines. However, in the experiments the probe superstrate is a factor of two closer to the main CPS line resulting in a larger perturbation.

The actual transmission line voltages and the voltages across the sampling probe gap are plotted in Fig. 11 for all investigated free-standing probe orientations and transmission line types. The perpendicular probe orientation results for both the MS and the CPS are similar to the on-wafer probe results, with a somewhat reduced bandwidth due to the increased probe parasitics. There is also a small, and for most applications inconsequential, delay introduced by the 8-μm probe tip length separating the probe gap from the main line. However, the probe in the parallel orientation with the MS line shows a roughly three-fold reduction in the measured signal amplitude caused by a strong direct coupling of the guided signal to the probe which bypasses the probe contact. This coupling is not seen for the CPS case, as also supported by the nearly negligible CPS loading observed in Fig. 10. The CPS guided mode appears as a differential signal between the conductors, and for closely-spaced conductors, the signal induced into the probe by one CPS conductor would be cancelled by the other. This may not be the case for wider CPS conductor spacings and/or for smaller probe-superstrate separations, possibly causing distortion. Such strong coupling

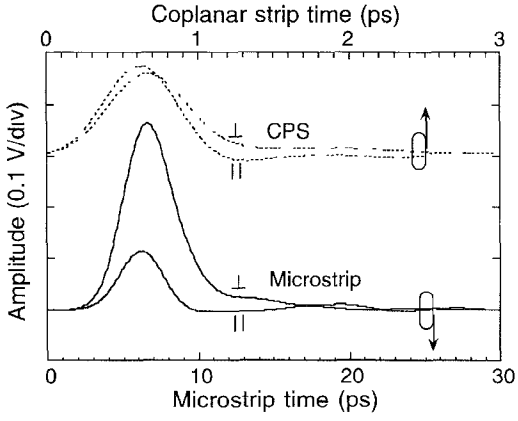

Fig. 12. Voltages generated by the free-standing probe on the MS (solid) and the CPS (dotted) lines under parallel and perpendicular probe orientations.

and orientation-dependent effects may hamper integrated circuit measurement applications. A possible solution is to orient the sampling probe structure normal to the circuit surface [16], or to shield the probe conductor. FD-TLM simulations may be used to explore various alternative designs.

The effectiveness of the free-standing probes at generating signals on the transmission lines is indicated in Fig. 12. The Gaussian current pulses generated by the PC switch gaps are 20 mA peak and 3.25 ps FWHM for the MS, and 12.5 mA peak and 0.5 ps FWHM for the CPS simulations. The transmission line voltages are calculated 34 μm and 16 μm from the probe edge for the MS and CPS lines, respectively. The signal generated at the parallel free-standing probe on the MS line shows a well-behaved response closely following the current waveform. Yet, the amplitude of the pulse is a factor of five lower than expected, which may be attributable to the coupling effects observed in the parallel probe MS measurements (Fig. 11). The signal generated at the perpendicular probe on the MS line shows an amplitude much closer to the expected due to the reduced coupling in analogy to the MS measurements (Fig. 11). However, there is a trailing shoulder present due to the increased mismatch between the structures. The signal generated on the CPS at the parallel probe closely follows the injected current shape, albeit with a lower than expected amplitude. The signal generated on the CPS at a perpendicular free-standing probe is similar to the signal generated via an on-wafer probe and shows a trailing positive shoulder. The formation of the positive trailing shoulder with approximately 10-ps duration after current injection from free-standing probes into CPS lines has also been observed experimentally [16], [18]. The injection efficiency is lower than expected due to the overall mismatch of the nonguiding probe and the CPS guiding-wave structures. However, it is similar to the on-wafer probe case, indicating that the additional free-standing probe parasitics do not degrade the performance.

IV. Summary

We have numerically investigated the performance of on-wafer and free-standing photoconductor probes for ultrafast signal measurement and generation. The photoconductor

probes have been applied to microstrip lines, as would be applicable for nearly 300 GHz bandwidth internal node measurements in microwave and millimeter-wave circuits. The performance of similar probes has also been characterized for ultrafast measurement applications on coplanar strip transmission lines capable of supporting terahertz-bandwidth signals. Parameters such as localized invasiveness, distributed loading, and the accuracy of waveform measurement have been analyzed. In general, the probes show a potential for subpicosecond time-resolution measurement and minimal localized invasiveness. However, the free-standing probe shows strong coupling effects to the microstrip line under parallel orientations that increase the distributed circuit loading and introduce uncertainty into the measured waveform amplitude. In addition, we have explored the applicability of the same probes for signal generation on transmission lines. For all cases, with a notable exception of the microstrip line with an on-wafer probe, the generation efficiency is compromised by the localized mismatches between the probe and the transmission line structures. The mismatches between the nonguiding probes and the guiding-wave lines also results in generated signal distortion exhibited as a positive trailing shoulder.

The results of this study show that care must be taken in applying free-standing probes for signal measurement and generation. For accurate measurements, coupling effects need to be eliminated either by proper probe orientation or by shielding. For clean signal generation, matched guiding-wave structures need to be used.

REFERENCES

[1] D. H. Auston, "Picosecond photoconductors: Physical properties and applications," in *Picosecond Electronic Devices*, C. H. Lee Ed. Orlando, FL: Academic Press, 1984.

[2] D. E. Cooper and S. C. Moss, "Picosecond optoelectronic measurement of the high-frequency scattering parameters of a GaAs FET," *IEEE J. Quant. Electron.*, vol. QE-22, pp. 94–100, Jan. 1986.

[3] S. L. Huang, E. A. Chauchard, C. H. Lee, H. A. Hung, T. T. Lee, and T. Joseph, "On-wafer photoconductive sampling of MMIC's," *IEEE Trans. Microwave Theory Tech.*, vol. 40, pp. 2312–2320, Dec. 1992.

[4] M. Matloubian, S. E. Rosenbaum, H. R. Fetterman, and P. T. Greiling, "Wide-band millimeter wave characterization of sub-0.2 micrometer gate-length AlInAs/GaInAs HEMT's," *IEEE Microwave Guided Wave Lett.*, vol. 1, pp. 32–34, Feb. 1991.

[5] W. J. Gallagher, C.-C. Chi, I. N. Duling, III, D. Grischkowsky, N. J. Halas, M. B. Ketchen, and A. W. Kleinsasser, "Subpicosecond optoelectronic study of resistive and superconductive transmission lines," *Appl. Phys. Lett.*, vol. 50, pp. 350–352, Feb. 1987.

[6] J. Kim, Y. J. Chan, S. Williamson, J. Nees, S. Wakana, J. Whitaker, and D. Pavlidis, "Novel high-impedance photoconductive sampling probe for ultra-high speed circuit characterization," in *Proc. IEEE GaAs IC Symp. Dig.*, Miami Beach, FL, 1992, pp. 19–22.

[7] J. Kim, J. Son, S. Wakana, J. Nees, S. Williamson, J. Whitaker, Y. Kwon, and D. Pavlidis, "Time-domain network analysis of mm-wave circuits based on a photoconductive probe sampling technique," in *Proc. IEEE MTT-S Int. Microwave Symp. Dig.*, Atlanta, GA, 1993, pp. 1359–1361.

[8] J. Kim, S. Williamson, J. Nees, S. Wakana, and J. Whitaker, "Photoconductive sampling probe with 2.3-ps temporal resolution and 4-μV sensitivity," *Appl. Phys. Lett.*, vol. 62, pp. 2268–2270, May 1993.

[9] T. Pfeifer, H. M. Heiliger, E. Stein von Kamienski, H. G. Roskos, and H. Kurz, "Fabrication and characterization of freely positionable silicon-on-sapphire photoconductive probes," *J. Opt. Soc. Am. B*, vol. 11, pp. 2547–2552, Dec. 1994.

[10] R. H. Voelker and R. J. Lomax, "A finite-difference transmission line matrix method incorporating a nonlinear device model," *IEEE Trans. Microwave Theory Tech.*, vol. 38, pp. 302–312, Mar. 1990.

[11] S. C. Moss, J. F. Knudsen, and D. D. Smith, "Linearity of response of ultrafast photoconductive switches: Critical dependence upon ion-implanatation and fabrication conditions," *J. Modern Opt.*, vol. 35, pp. 2007–2030, Dec. 1988.

[12] V. Pasiskevicius, A. Deringas, and A. Krotkus, "Photocurrent nonlinearities in ultrafast optoelectronic switches," *Appl. Phys. Lett.*, vol. 63, pp. 2237–2239, Oct. 1993.

[13] M. Y. Frankel, R. H. Voelker, and J. N. Hilfiker, "Coplanar transmission lines on thin substrates for high-speed low-loss propagation," *IEEE Trans. Microwave Theory Tech.*, vol. 42, pp. 396–402, Mar. 1994.

[14] I. J. Bahl, "Transmission lines," in *Handbook of Microwave and Optical Components*, K. Chang, Ed. New York: Wiley, 1989.

[15] M. Y. Frankel, S. Gupta, J. A. Valdmanis, and G. A. Mourou, "Terahertz attenuation and dispersion characteristics of coplanar transmission lines," *IEEE Trans. Microwave Theory Tech.*, vol. 39, pp. 910–916, June 1991.

[16] D. R. Dykaar and S. B. Darack, "Simple technique for picosecond electrical pulse injection into arbitrary circuits," *Appl. Phys. Lett.*, vol. 65, pp. 2525–2526, Nov. 1994.

[17] M. Y. Frankel, "500-GHz characterization of an optoelectronic S-parameter test structure," *IEEE Microwave Guided Wave Lett.*, vol. 4, pp. 118–120, Apr. 1994.

[18] T. Pfeifer, H.-M. Heiliger, H. G. Roskos, and H. Kurz, "High-frequency on-wafer testing with freely positionable silicon-on-sapphire photoconductive probes," to appear in *Proc. IEEE MTT-S Int. Microwave Symp. Dig.*, Orlando, FL, 1995.

Robert H. Voelker (S'81-M'90-SM'95) was born in Midland, MI. He received the B.S.E. (summa cum laude, 1982), the M.S.E. (1983), and the Ph.D. (1989) degrees in electrical engineering from the University of Michigan, Ann Arbor.

Since 1990, he has been an Assistant Professor of electrical engineering at the University of Nebraska-Lincoln (UNL), where he teaches courses in analog and digital VLSI design, active filters, electromagnetics, and electronics. As a member of the Center for Electro-Optics at UNL, his research interests include computer-aided design of high-speed/high-frequency integrated circuits and their interconnections, and supercomputing.

Dr. Voelker was an IBM Graduate Fellow for the 1983–1984 academic year and a Shell Doctoral Fellow for the 1984–1987 academic years, and he held a U.S. Army Research Office Fellowship for the 1987–1989 academic years. He is a member of Tau Beta Pi, Eta Kappa Nu, and the American Society for Engineering Education.

Michael Y. Frankel was born in St. Petersburg, Russia, in 1964. He received the B.S. degree (magna cum laude) from the University of Maryland, College Park, in 1986, the M.S. degree from the University of Rochester, NY, in 1988, and the Ph.D. degree from the University of Michigan, Ann Arbor, in 1991, all in electrical engineering.

He is currently with the Optical Sciences Division, Naval Research Laboratory. His interests are in ultra-fast optoelectronic studies and modeling of semiconductor materials, high-speed transmission lines, photodetectors, and transistors. He is also actively involved in developing fiber-optic components and control methods for phased-array radars. He has over 30 publications and conference presentations in these areas and holds two patents.

Christopher G. Sentelle received the B.S. degree in electrical engineering from the University of Nebraska-Lincoln (UNL) in December 1993. He is currently a 2nd Lieutenant in the US Air Force and is completing the M.S. degree in electrical engineering at UNL. His thesis topic is FD-TLM electromagnetic field simulation of high-speed integrated circuits utilizing superconducting Josephson junction devices and resonant tunneling diodes.

Lt. Sentelle is a member of Eta Kappa Nu.